Comparison of SVSF-KF Adaptive Estimation Algorithms on an Electrohydrostatic Actuator Subject to a Fault

Jacob Goodman, Waleed Hilal, *Student Member, IEEE*, Stephen A. Gadsden Sr., *Member, IEEE*, and Charles D. Eggleton

***Abstract*—State estimation strategies are vital for obtaining knowledge of a dynamic system's state when faced with limited measurement capability, sensor noise, or uncertain system dynamics. The Kalman filter (KF) is one of the most widely recognized filters and provides the optimal solution for linear state estimation problems. The smooth variable structure filter (SVSF) is a model-based strategy that is also formulated as a predictor-corrector. Despite being a suboptimal estimator, the SVSF is highly robust to modeling uncertainties, errors, and system change. The combination of the SVSF with the KF (SVSF-KF) results in an adaptive estimation algorithm that provides an optimal KF estimate in normal operating conditions, and a robust SVSF estimate in the presence of faults or uncertainties. While effective in some cases, the SVSF-KF has been shown to suffer from several drawbacks associated with the time-varying smoothing boundary layer (SBL) and adaptive gain used to detect system change. Several new approaches have been proposed in recent years with the aim of improving the SVSF-KF's performance. Among these approaches is a novel gain formulation based on the normalized innovation squares (NISs), while another makes use of the interacting multiple model (IMM) framework. In this article, we review the newly proposed SVSF-KF formulations and compare their performance on an electrohydrostatic actuator (EHA) test case.**

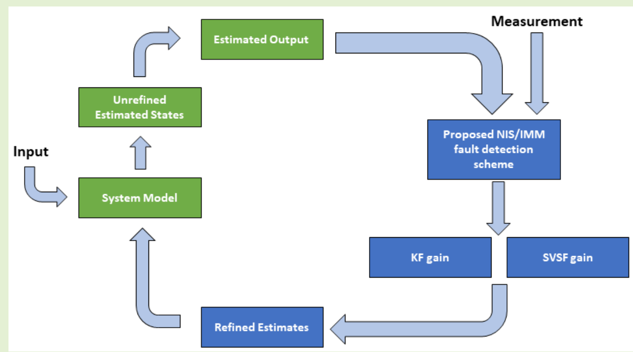

***Index Terms*—Adaptive filtering, estimation theory, hydrostatic actuator, interacting multiple models (IMMs), Kalman filter (KF), smooth variable structure filter (SVSF).**

I. Introduction

STATE estimation strategies are required to obtain information about a dynamic system's state when sensor measurements can only provide a noisy and limited picture. The Kalman filter (KF), introduced in the early 1960s [1], revolutionized the field of estimation theory by providing the optimal solution to the linear stochastic estimation problem [2]. The KF has led to many important engineering achievements in navigation, control, space flight, and other areas [3], [4], [5].

The KF requires a linear mathematical model of the system along with knowledge of its measurement and process noise characteristics. The KF also assumes that both the process and measurement noise are zero-mean and have a Gaussian distribution, otherwise known as white. When these conditions are met, the KF provides the online optimal estimate of the states that minimizes the mean square error [2], [6], [7], [8]. Significant development effort has been directed toward the KF, with improvements to numerical stability, extensions to nonlinear systems, and many other enhancements [9], [10], [11].

In many real systems, a priori information about the underlying dynamics and noise is not known—or known only to a limited degree. In addition, systems can undergo sudden changes and exhibit new dynamic characteristics—either because they intrinsically operate in more than one mode, or due to unexpected parameter changes or faults. The KF as well as other estimators can often struggle in these situations,

Received 25 February 2024; accepted 19 August 2024. Date of publication 27 November 2024; date of current version 14 January 2025. The associate editor coordinating the review of this article and approving it for publication was Dr. Olga Fink. *(Corresponding author: Waleed Hilal.)*

Jacob Goodman was with the Department of Mechanical Engineering, University of Maryland, Baltimore County, MD 21250 USA. He is now with the John Hopkins University Applied Physics Laboratory, Laurel, MD 20723 USA (e-mail: jg4@umbc.edu).

Waleed Hilal and Stephen A. Gadsden Sr. are with the Intelligent and Cognitive Engineering (ICE) Laboratory, McMaster University, Hamilton ON L8S 4L8, Canada (e-mail: hilalw@mcmaster.ca; gadsden@mcmaster.ca).

Charles D. Eggleton is with the Department of Mechanical Engineering, University of Maryland, Baltimore County, MD 21250 USA (e-mail: eggleton@umbc.edu).

Digital Object Identifier 10.1109/JSEN.2024.3452488

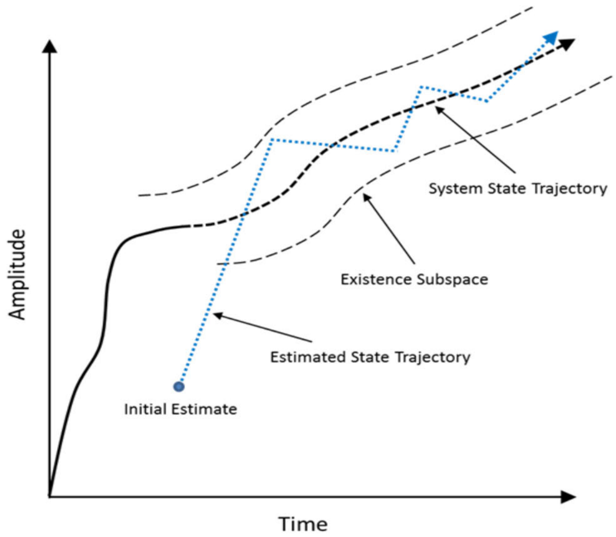

Fig. 1. Basic concept of the sliding boundary layer in SVSF [12], [20].

as their underlying mathematical representation of the system is rendered inaccurate [12].

Robust and adaptive estimation techniques are specifically designed for cases where system dynamics are uncertain or may be subject to change. Robust estimation techniques include the robust KF [13], H∞ methods [14], [15], variable structure techniques [16], [17], [18], and others. In robust estimation, the goal is to render the filter as resilient as possible to modeling uncertainties. Adaptive estimation attempts to adjust the underlying filter dynamically in response to modeling uncertainty and system change. Adaptive techniques include online parameter estimation, automatic tuning of noise parameters, gain adjustment techniques, and multiple model methods [6], [7], [19], [20]. In multiple model methods, the system is assumed to operate in one or more modes from a set of different possible modes, with different frameworks for choosing between and weighting the different modes.

A robust estimation algorithm termed the smooth variable structure filter (SVSF) was proposed in 2007 [18]. The SVSF is based on variable structure theory and sliding mode concepts [21], [22], [23]. The SVSF uses a nonlinear switching gain to drive the estimated states to a region around the true states, termed the "existence subspace." The width of this subspace is unknown and varies with time—depending on the underlying system and measurement uncertainties. If an upper bound on these uncertainties can be determined, an upper bound on the existence subspace can be calculated [18]. The SVSF is not an optimal filter; however, it is highly robust to modeling uncertainties and system change [24], [25]. A significant amount of research has been based on the SVSF's robustness to the presence of faulty conditions [18], [24], [25], [26], [27], [28]. Fig. 1 illustrates the basic SVSF concept.

Due to the nature of the SVSF's switching gain, an artificial noise known as chattering is introduced. While chattering is observed both in the a priori and a posteriori estimates [29], the a posteriori estimate is highly sensitive to the measurement noise—with the estimated state converging to the measured state. To limit these effects, a smoothing boundary layer (SBL) is introduced such that estimated states within the SBL are interpolated based on the ratio of the SBL width to the a priori measurement error [24]. Outside the SBL, the full nonlinear switching action is applied to ensure the stability of the estimation process. By adjusting the SBL width, one can control the overall smoothness of the estimate. Too large of an SBL can result in filter divergence, while if too small, renders the estimates sensitive to measurement noise [18], [24], [28], [29].

The SVSF has been the subject of significant development over the years, with numerous advancements. Some examples include the derivations of a covariance term [28], [30], several approaches to a time-varying SBL (VBL) [28], [29], [31], [32], new methods to deal with missing measurements [29], the derivation of a continuous-time SVSF, a square root SVSF formulation [33], [34], a second-order SVSF formulation [26], [35], [36], [37], as well as many other enhancements and applications [27], [38], [39], [40], [41], [42], [43], [44], [45], [46], [47], [48], [49], [50], [51], [52], [53], [54], [55], [56], [57], [58], [59], [60].

One particular development is the SVSF with the KF (SVSF-KF) [28]. The SVSF-KF is an adaptive hybrid estimation strategy that attempts to provide the KF estimate during normal system operation and the SVSF during a fault. The SVSF-KF represents a powerful paradigm for many common applications. A properly tuned KF can be designed for optimal estimation during normal system operation, with the robust SVSF being available as a backup during faults or system changes [61], [62], [63], [64].

The original SVSF-KF strategy emerged from the derivation of an optimal VBL [31]. It was discovered that integration of the optimal VBL into the SVSF gain reduces the SVSF to the KF [21], [28]. As a result, a hybrid adaptive gain switching approach was proposed using the VBL as an indicator of system change. During normal operation of the filter, the VBL converges to a width related to the overall assumed process noise. During a fault, however, the VBL begins to grow. A threshold approach based on the VBL was used to switch between the KF gain and the SVSF gain. This approach was shown to be effective in several cases, and multiple nonlinear extensions of the strategy have been put forward [28], [37], [47].

In some of our related studies [65], we demonstrated that the VBL may not always be the best mechanism for system change detection. The overall VBL width is highly coupled to the recent state estimate, such that when the SVSF gain is activated in the presence of a fault, the VBL width will drop well below the triggering threshold at the next timestep. This results in the filter using the KF gain instead of the SVSF gain, despite the continued fault condition.

We have put forth three alternative approaches to the SVSF-KF algorithm that we believe solve these problems and can offer superior performance. The simplest approach keeps the adaptive gain switching structure of the SVSF-KF and exchanges the VBL with a fading memory average of the normalized innovation square (NIS), combined with a hysteresis style threshold approach. The NIS are commonly used for monitoring system change [2], [6], [19], [66], [67] and represent a simple and effective alternative to the VBL. We have called this method the NIS SVSF-KF, which in essence, makes use of a threshold-style approach to determining the presence or absence of a fault. In our second two methods, we have opted for a multiple model approach. In the first of these two methods, we use the framework of the multiple model adaptive estimator (MMAE) [7], [20], [26], [68], which takes a Bayesian approach to coordinate weighting between two independent filters running in parallel – in our case, the SVSF and KF. The second approach uses the framework of the interacting multiple model (IMM) estimator [19], [24], [68], which despite being more complex, has greater dynamic capability. The two versions have been termed the MMAE SVSF-KF and IMM SVSF-KF, respectively. Both the MMAE and IMM approaches make use of a weighting strategy to output estimates which are comprised of a weighted combination of the filters running in parallel, as opposed to a threshold approach like the NIS.

In this article, we seek to compare the performance of all the SVSF-KF methods in a simulated electrohydrostatic actuator (EHA) scenario. The EHA is a relatively new system that uses a variable speed pump and associated hydraulics to drive an actuator. The EHA has impressive performance characteristics, capable of submicrometer control of loads in the 20-kg range [18], [36], [69], [70], [71]. Much of the academic research into the SVSF has used the EHA as a benchmark test case to demonstrate performance—particularly under various fault regimes [18], [27], [29], [36], [40], [46], [48].

The novelty of this study lies in the fact that we extend upon our previous studies in [72] by applying the proposed SVSF-KF formulations on a real-life nonlinear experimental setup: the EHA. Previously, the proposed SVSF-KF formulations have only been demonstrated on a simple linear system such as a damped harmonic oscillator. In those previous studies, the fault cases covered were not as extensive as those covered in our study. Furthermore, this study covers a wider range of formulations, such as statistical-based hard thresholding with the NIS, and mixed probability models such as the MMAE and IMM formulations. Overall, the methods proposed in this study, as will be demonstrated throughout this article, result in improved fault detection capabilities and overall performance compared to all previous studies on the topic. Furthermore, it will be demonstrated within this study that several limitations associated with the SVSF-KF formulations can be addressed by the proposed thresholding models, especially that of the high-frequency switching or "chattering" problem.

This article is organized as follows. Section II provides a brief overview of the SVSF with covariance and the original SVSF-KF. In Section III, we outline the three new SVSF-KF methods for implementation in the EHA simulations. In Section IV, we provide a detailed overview of the experimental simulations and implementation of the EHA and SVSF-KF methods. The results of the simulation are highlighted and discussed in Section V. Finally, in Section VI, we present the overall conclusions of this research.

II. Review of the SVSF and SVSF-KF

The linear system model and measurement model of the SVSF can be seen in (1), where $\boldsymbol{A}$ is the system model matrix, $\boldsymbol{B}$ is the input matrix, $\boldsymbol{w}_k$ is the system model noise, $\boldsymbol{x}$ is the state of the system, and k is the current timestep [17]

$$\boldsymbol{x}_{k+1} = \boldsymbol{A}\boldsymbol{x}_k + \boldsymbol{B}\boldsymbol{u}_k + \boldsymbol{w}_k. \tag{1}$$

Nonlinear systems can be expressed as follows in (2), provided that the system of interest is differentiable and observable:

$$\boldsymbol{x}_{k+1} = \mathfrak{F}(\boldsymbol{x}_k, \boldsymbol{u}_k, \boldsymbol{w}_k). \tag{2}$$

In either case, the measurement equation must be linear and of full rank, and can be seen as follows in (3), where $\boldsymbol{H}$ is the measurement matrix, $\boldsymbol{v}$ is the measurement noise, and $\boldsymbol{z}$ is the system measurement:

$$\boldsymbol{z}_k = \boldsymbol{H}\boldsymbol{x}_k + \boldsymbol{v}_k. \tag{3}$$

Reduced order methods, or artificial measurements, can be used to generate a complete measurement matrix if needed [18], [24], [28]. For the SVSF covariance calculations, a linear system of the form (1) is required. For nonlinear systems, various techniques used for nonlinear Kalman filtering can be adapted, such as the extended KF (EKF) and unscented KF (UKF) [73].

The steps and equations that form the SVSF algorithm are presented below [28]. Note that there are several differences in this version of the SVSF, compared to the original—compared to the originalwhich does not include a covariance. First, an a priori state estimate is determined using an approximate system model $\hat{\mathfrak{F}}$ and the previous a posteriori (or initial) state estimate. The estimated a priori measurements $\hat{\boldsymbol{z}}_{k+1|k}$ are then calculated

$$\hat{x}_{k+1|k} = \hat{\mathfrak{F}}(\hat{\boldsymbol{x}}_{k|k}, \boldsymbol{u}_k) \tag{4}$$
$$\hat{z}_{k+1|k} = \hat{H}\hat{x}_{k+1|k}. \tag{5}$$

The error of the estimated a priori measurements can then be calculated by

$$\boldsymbol{e}_{z_{k+1|k}} = \boldsymbol{z}_k - \hat{\boldsymbol{z}}_{k+1|k}. \tag{6}$$

The SVSF gain, $\boldsymbol{K}_{k+1}$, is calculated based on the error of the a priori and a posteriori state estimates. Thus, the *a priori* state estimate is updated to the a posteriori state estimate using the SVSF gain

$$\hat{\boldsymbol{x}} = \hat{\boldsymbol{x}}_{k+1|k} + \boldsymbol{K}_{k+1}\boldsymbol{e}_{z_{k+1|k}}. \tag{7}$$

The SVSF gain, which is derived based on a Lyapunov condition which ensures the stability of the estimation process, can be expressed as follows:

$$\boldsymbol{K}_{k+1} = \hat{\boldsymbol{H}}^{+}\text{diag}\left[\left(\gamma\left|\boldsymbol{e}_{z_{k|k}}\right| + \left|\boldsymbol{e}_{z_{k+1|k}}\right|\right) \circ sat\left(\boldsymbol{e}_{z_{k+1|k}}, \boldsymbol{\Psi}\right)\right] \times \left[\text{diag}\left(\boldsymbol{e}_{z_{k+1|k}}\right)\right]^{-1} \tag{8}$$

where $^{+}$ denotes the pseudoinverse, and $\circ$ denotes the Schur product. γ is a diagonal scalar matrix such that $0 < \gamma_{ii} < 1$. Note the saturation term; for a priori errors smaller than the SBL width $\boldsymbol{\Psi}$, the SVSF gain is interpolated. If the a priori error grows outside this bound, the full nonlinear switching gain is used. The saturation function can be defined element-wise for a given error vector $\boldsymbol{e}$ and SBL width $\boldsymbol{\Psi}$ as [18]

$$sat_i(\boldsymbol{e}, \boldsymbol{\Psi}) = \begin{cases} (e_i/\psi_i), & \text{for} |e_i/\psi_i| \leq 1 \\ sign(e_i/\psi_i), & \text{for} |e_i/\psi_i| > 1. \end{cases} \tag{9}$$

The a priori and a posteriori covariances, $\boldsymbol{P}$, can be calculated at the same time, as the SVSF estimation process does not intrinsically require a covariance. In the following equations, $\boldsymbol{I}$ is the identity matrix, $\boldsymbol{Q}$ is the system noise covariance, and $\boldsymbol{R}$ is the measurement noise covariance:

$$\boldsymbol{P}_{k+1|k} = \boldsymbol{A}\boldsymbol{P}_{k|k}\boldsymbol{A}^T + \boldsymbol{Q}_k \tag{10}$$

$$\boldsymbol{P}_{k+1|k+1} = (\boldsymbol{I} - \boldsymbol{K}_{k+1}\boldsymbol{H})\boldsymbol{P}_{k+1|k}(\boldsymbol{I} - \boldsymbol{K}_{k+1}\boldsymbol{H})^T + \boldsymbol{K}_{k+1}\boldsymbol{R}\boldsymbol{K}_{k+1}^T. \tag{11}$$

The a priori measurements are then updated to the a posteriori measurement by

$$\hat{z}_{k+1|k+1} = \hat{\boldsymbol{H}}\hat{\boldsymbol{x}}_{k+1|k+1}. \tag{12}$$

Subsequently, the error of the a priori estimate is updated to the a posteriori error. The process then repeats iteratively

$$\boldsymbol{e}_{z_{k+1|k+1}} = z_k - \hat{z}_{k+1|k+1}. \tag{13}$$

In the VBL strategy proposed in [28], the SVSF covariance is used to determine an optimal SBL width at each timestep. Using the form of the SVSF gain expressed in (8), and considering only the region within the saturation limits, the SVSF gain can also be written as

$$\boldsymbol{K} = \boldsymbol{H}^{-1}\bar{\boldsymbol{A}}\boldsymbol{\Psi}^{-1} \tag{14}$$

where

$$\bar{\boldsymbol{A}} = \text{diag}\left[\left(\gamma\left|\boldsymbol{e}_{z_{k|k}}\right| + \left|\boldsymbol{e}_{z_{k+1|k}}\right|\right)\right]. \tag{15}$$

Using the gain in the form of (14), the proposed optimal VBL width is one which minimizes the trace of the a posteriori covariance at each timestep. This was determined to be [28]

$$\boldsymbol{\Psi} = \left(\frac{\bar{\boldsymbol{A}}^{-1}\boldsymbol{H}\boldsymbol{P}_{k+1|k}\boldsymbol{H}^T}{\boldsymbol{H}\boldsymbol{P}_{k+1|k}\boldsymbol{H}^T + \boldsymbol{R}}\right)^{-1}. \tag{16}$$

The VBL directly implemented in the SVSF results in a reduction to the KF; however, the VBL nonetheless provides a useful indication of a system fault. During normal operation, the VBL generally converges to a size proportional to the amount of assumed process noise. In the presence of a system change, the VBL will rapidly expand. The original SVSF-KF exploits this feature to detect system changes. During normal operation, the VBL is expected to remain bound within a fixed region, and the KF gain is used. In the presence of a system change, the VBL will begin to grow beyond this bound, and the estimator switches to the SVSF gain. In setting up the filter, the designer chooses a fixed VBL threshold that will achieve the desired detection. However, as discussed, the use of the VBL can result in inconsistent and unstable switching between the KF and SVSF gain, resulting in poor performance [65]. Furthermore, we refer the reader to [18] and [21], [22], [23], for an overview of the guarantees for nonsingularity of the SVSF.

III. Proposed SVSF-KF Approaches

A. Normalized Innovation Square SVSF-KF

The innovation and innovation covariance are names for two important terms that appear in many recursive estimators such as the KF and SVSF (with covariance). The innovation $\boldsymbol{\nu}$ represents the difference between the actual measurements and the a priori estimate of the measurements. The innovation covariance $\boldsymbol{S}$ characterizes the uncertainty in the measurement predictions, as shown in the following equation:

$$\boldsymbol{\nu}_{k+1} = z_k - \boldsymbol{H}\boldsymbol{A}\hat{\boldsymbol{x}}_{k+1|k} \tag{17}$$

$$\boldsymbol{S}_{k+1} = \boldsymbol{H}\boldsymbol{P}_{k+1|k}\boldsymbol{H}^T + \boldsymbol{R}_{k+1}. \tag{18}$$

The NIS SVSF-KF, as shown below in (19), uses the square innovation vector at a given timestep, normalized by the innovation covariance to detect system change

$$\boldsymbol{r_k} = \boldsymbol{\nu}_k^T \boldsymbol{S}_k^{-1} \boldsymbol{\nu}_k. \tag{19}$$

In a properly modeled system, under the assumption of white Gaussian noise, a KF's innovations have several important statistical properties, namely that they are white, have zero mean, and have a known covariance [2]. When the filter model fails to match the reality, the innovations will violate these conditions, and in many cases, begin to grow. As a result, the innovations are often used to detect filter divergence [6], [8], [19].

For improved robustness, a sequence of the innovation history can be averaged using a fading memory technique. This will help smooth out any noise in the innovations and avoid false detections. In addition, to avoid an erratic switching effect across a single threshold line, two thresholds with a hysteresis approach can be arranged: a higher "on" threshold such that false triggers of the SVSF are avoided, and a lower "off" threshold, to be triggered once the innovations drop back to normal.

The fading memory average of the NIS can be expressed in (20) below as $\boldsymbol{r_k^\alpha}$ [28]. The weights are determined by a memory factor α where $0 < \alpha < 1$, such that more distant innovations are exponentially weighted lower

$$\boldsymbol{r_k^\alpha} = \alpha \boldsymbol{r_{k-1}^\alpha} + \boldsymbol{r_k}. \tag{20}$$

In an optimally modeled filter, the distribution of fading memory average of the NIS can be modeled as approximately chi-squared with a number of degrees of freedom related to the number of samples N, and α as follows [19]:

$$dof\,\chi = \frac{N}{1-\alpha}. \tag{21}$$

The thresholds can then be defined based on an appropriate chi-squared tail probability. For example, a system with three states and a memory factor of $\alpha = 0.98$, will result in an expected chi-squared distribution with 150 degrees of freedom. A tail probability of 0.001, reflecting an unexpected innovation sequence, would translate into an "on" threshold of about 210.

B. Multiple Model Adaptive Estimator SVSF-KF

In the MMAE approach, a set of filters are run independently and in parallel with each other. Each of the filters' innovations and innovation covariances are used to calculate a Gaussian likelihood. Using a Bayesian framework, one can assign a probability to each filter based on these likelihoods. The MMAE provides a weighted sum of the individual filter estimates as its final estimate. The MMAE SVSF-KF takes this essential approach, using the KF and SVSF as the two filters, yet both with the same internal models.

In the MMAE approach, the innovation and innovation covariance of each individual filter is used to compute a Gaussian likelihood $f_{(i),k}$ for each of i filters out of a set of m filters as shown in (22) [2], [19]

$$f_{(i),k} = \frac{1}{\sqrt{\det\left(2\pi \left|\boldsymbol{S}_{(i),k}\right|_{ABS}\right)}} \exp\left[-\frac{1}{2}\boldsymbol{\upsilon}_{(i),k}\boldsymbol{S}_{(i),k}^{-1}\boldsymbol{\upsilon}_{(i),k}\right]. \quad (22)$$

Probabilities for each individual filter out of the total set of filters can then be computed by the following equation:

$$p_{(i),k} = \frac{f_{(i),k}\, p_{(i),k-1}}{\sum_{i=2}^{r} f_{(i),k}\, p_{(i),k-1}}. \quad (23)$$

The MMAE uses the computed probabilities to provide a final weighted output estimate as shown in (24) below. Note that the MMAE will require an initial probability for each filter

$$\hat{\boldsymbol{x}}_{\text{MMAE},k+1} = \sum_{i=2}^{m} \hat{\boldsymbol{x}}_{(i),k}\, p_{(i),k}. \quad (24)$$

One noted disadvantage of the MMAE is that it is better suited to static systems [19], [20]. The MMAE generally will converge to the most probable filter model with good results. If, however, the system exhibits a switching behavior, the MMAE can struggle to follow the mode transitions after having converged fully to a prior mode.

To mitigate these effects in the case of the MMAE SVSF-KF, several ad hoc modifications are made. An artificial lower bound on the individual filter probabilities is set, so no one individual filter probability goes to zero. In addition, upon switching to the SVSF estimate, the internal KF estimate is reset using the SVSF state estimate and initial covariance. This affords the opportunity for the MMAE SVSF-KF to eventually switch back to the KF estimate following a system's return to normal operation. To avoid unwanted excessive switching while an actual fault is present, a counter can be used so that the resetting action is only executed after a designer-specified interval.

C. Interacting Multiple Model SVSF-KF

In the IMM SVSF-KF, we use the IMM framework [19] to coordinate between the KF and SVSF estimate. In a typical IMM approach, multiple system and noise models are defined across the range of possible system behavior. The IMM assumes that the transition from one system mode to another is a Markov process with known, time-invariant, mode transition probabilities. A principal advantage of the IMM is its ability to dynamically identify and switch to the most likely system modes [19].

The IMM algorithm has five basic steps to its recursion, followed by a final output update [19], [28], [74]. First, the mixing probabilities $\mu_{i|j,k|k}$ are calculated by (25) – i.e., the probability that the system was in mode M_i at the previous timestep and in mode M_j at the current timestep, where $i, j = 1, \ldots, m$ for m number of possible modes

$$\mu_{i|j,k|k} = \frac{1}{\bar{c}_j} p_{ij}\mu_{i,k} \quad (25)$$

$$\bar{c}_j = \sum_{i=1}^{m} p_{ij}\mu_{i,k} \quad (26)$$

where p_{ij} is the mode transition probabilities, $\mu_{i,k}$ is the mode probability from the previous timestep, and $\bar{c}_j$ is a normalizing constant.

Then, the mixing probabilities are used to calculate the mixed initial conditions for the state estimate and covariance

$$\hat{x}_{0j,k|k} = \sum_{i=1}^{m} \hat{x}_{i,k|k}\mu_{i|j,k|k} \quad (27)$$

$$\hat{P}_{0j,k|k} = \sum_{i=1}^{m} \mu_{i|j,k|k}\left\{\hat{P}_{i,k|k} + \left(\hat{x}_{i,k|k} - \hat{x}_{0j,k|k}\right)\left(\hat{x}_{i,k|k} - \hat{x}_{0j,k|k}\right)^T\right\} \quad (28)$$

where $\hat{x}_{i,k|k}$ and $\hat{P}_{i,k|k}$ are the mode-matched state and covariance estimate from the previous timestep.

The initial conditions are then used for mode-matched filtering – they are used as inputs to each individual filter along with the current measurement $\boldsymbol{z}_k$ and input $\boldsymbol{u}_k$. Each filter provides an updated mode-matched state and covariance estimate, $\hat{x}_{i,k+1|k+1}$ and $\hat{P}_{i,k+1|k+1}$, respectively.

A likelihood function based on the Gaussian assumption is defined for each filter, based on the mode-matched innovation and innovation covariance

$$\Lambda_{j,k+1} = \mathcal{N}\left(z_k; \boldsymbol{\upsilon}_{j,k+1}, \boldsymbol{S}_{j,k+1}\right) \quad (29)$$

which can be computed as follows [2], [19]:

$$\Lambda_{j,k+1} = \frac{1}{\sqrt{\det\left(2\pi \left|\boldsymbol{S}_{j,k+1}\right|_{ABS}\right)}} \exp\left[-\frac{1}{2}\boldsymbol{\upsilon}_{j,k+1}\boldsymbol{S}_{j,k+1}^{-1}\boldsymbol{\upsilon}_{j,k+1}\right]. \quad (30)$$

The computed likelihoods are used to update the mode probabilities

$$\mu_{j,k+1} = \frac{1}{c}\Lambda_{j,k+1}\bar{c}_j \quad (31)$$

$$c = \sum_{i=1}^{m} \Lambda_{j,k+1}\bar{c}_j. \quad (32)$$

Finally, the output state and covariance are updated as a weighted sum of the mode-matched estimates and associated mode probabilities as follows:

$$\hat{x}_{k+1|k+1} = \sum_{j=1}^{m} \hat{x}_{j,k+1|k+1}\mu_{j,k+1} \quad (33)$$

$$\hat{P}_{k+1|k+1} = \sum_{j=1}^{m} \mu_{j,k+1}\left\{\hat{P}_{j,k+1|k+1} + \left(\hat{x}_{j,k+1|k+1} - \hat{x}_{k+1|k+1}\right)\left(\hat{x}_{j,k+1|k+1} - \hat{x}_{k+1|k+1}\right)^T\right\}. \quad (34)$$

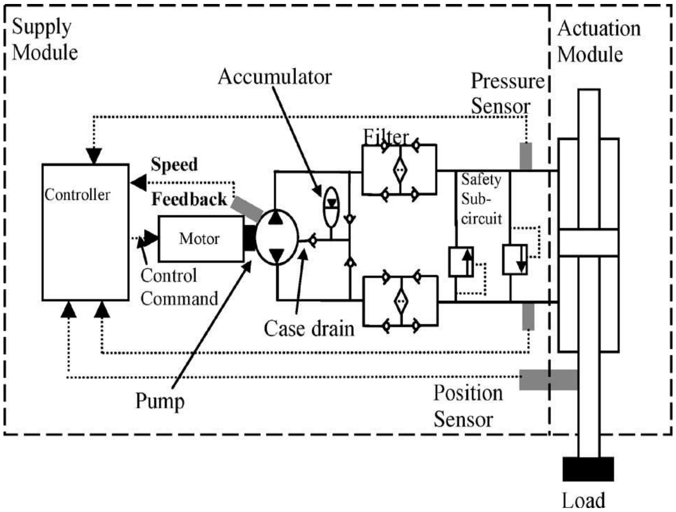

Fig. 2. Sample schematic of the EHA under study.

In the IMM SVSF-KF, the two modes are, to reiterate, the KF and SVSF. Unlike typical IMM implementations, however, both filters use the same essential model and noise statistics. The intrinsic distinctions in performance between the two filters in cases of normal operation versus a fault allow the IMM to identify the more likely filter.

IV. Experimental Simulations

For the purposes of demonstrating and comparing the different SVSF-KF algorithms, we shall examine the electro-hydrostatic actuator problem, one of the popular benchmark problems for the SVSF. The EHA is a high-performance actuation system that uses an electric variable-speed bidirectional pump to propel hydraulic oil into or out of two chambers on either end of a piston within a hydraulic cylinder. The resulting pressure differences drive the movement of a shaft and load coupled to the piston. By controlling motor/pump speed and direction, extremely high precision (submicrometer) control of even large (∼20 kg) loads can be achieved [18]. A schematic of the EHA under study can be seen in Fig. 2.

Based on theoretical considerations and experimental studies [70], and using the parameter definitions and values in Table I, the following third-order transfer function can be used to model the EHA dynamics [18]:

$$\frac{x(s)}{u(s)} = \frac{\frac{2D_p\beta_e A_E}{MV_0}}{s^3 + s^2\left(\frac{B_E}{M} + \frac{L}{V_0}\beta_e\right) + s\left(\frac{2\beta_e A_E^2}{MV_0}\right)}. \tag{35}$$

In [18], a discrete time state space model for the EHA was presented based on a measurement interval of 1 ms. This model represents three states of the EHA's output actuator, position, velocity, and acceleration as follows:

$$x_1 = x \tag{36}$$

$$x_2 = \frac{dx}{dt} \tag{37}$$

$$x_3 = \frac{d^2x}{dt^2}. \tag{38}$$

TABLE I
Parameter Values for the EHA Transfer Function

Symbol	Quantity	Value
D_p	Pump Displacement	1.69×10^{-7} m^3/rad
β_e	Effective Bulk Modulus	1.5×10^8 to 2×10^8 Pa
A_E	Piston Area	5.05×10^{-4} m^2
M	Load mass	20 Kg
V_0	Chamber volume	6.85×10^{-5} m^3
B_E	Load friction	760 $N\,s/m$
L	Leakage Coefficient	2.5×10^{-11} m^3/Pa - s

Two models were presented, one for normal EHA operation ($\boldsymbol{A_1}$), and the other reflecting modeling uncertainty ($\boldsymbol{A}_2$). We shall use these system models in our simulations to reflect normal operation and sudden system changes. The modeling uncertainty that arises in this experiment is attributed to simulated sudden changes in the parameter values of the EHA, as outlined in Table I [28]. While this is an artificially simulated scenario, the possible faults or uncertainties that may occur in practice can exhibit similar effects to the approach we are adopting to simulating such adverse effects

$$\boldsymbol{A_1} = \begin{bmatrix} 1 & 0.001 & 0 \\ 0 & 1 & 0.001 \\ -557.02 & -28.616 & 0.9418 \end{bmatrix} \tag{39}$$

$$\boldsymbol{B} = \begin{bmatrix} 0 \\ 0 \\ 557.02 \end{bmatrix} \tag{40}$$

$$\boldsymbol{A}_2 = \begin{bmatrix} 1 & 0.001 & 0 \\ 0 & 1 & 0.001 \\ -240 & -28 & 0.9418 \end{bmatrix}. \tag{41}$$

We assume process and measurement noise sequences, $\boldsymbol{w}$ and $\boldsymbol{v}$, in our simulations to be Gaussian, zero mean, and defined by the following covariance matrices, respectively [28]:

$$\boldsymbol{Q} = \begin{bmatrix} 1\times10^{-5} & 0 & 0 \\ 0 & 1\times10^{-3} & 0 \\ 0 & 0 & 1\times10^{-1} \end{bmatrix} \tag{42}$$

$$\boldsymbol{R} = \begin{bmatrix} 1\times10^{-4} & 0 & 0 \\ 0 & 1\times10^{-2} & 0 \\ 0 & 0 & 1 \end{bmatrix}. \tag{43}$$

All filters are provided with the same values of $\boldsymbol{Q}$ and $\boldsymbol{R}$. The initial covariance $\boldsymbol{P}_0$ was set to $10\boldsymbol{Q}$. The system shall be excited by a Gaussian random input sequence with amplitudes normalized between -1 and 1 rad/s.

The SVSF estimate uses a filter convergence rate of $\gamma = 0.1$ and a fixed SBL width defined as

$$\boldsymbol{\Psi} = \begin{bmatrix} 0.05 \\ 0.5 \\ 5 \end{bmatrix} \tag{44}$$

which is determined based on the overall distribution of the measurement noises [28]. For the SVSF-KF, the VBL limit was set to 0.3 and based on the position estimate. This value was determined by an initial trial and error analysis of the VBL response to the fault.

For the NIS SVSF-KF, the memory factor α was set to 0.98. Per (21), this means the nonfault NIS should have an approximate chi-squared distribution with 150 degrees of freedom. The values of 210 for the "on" threshold and 180 for the "off" threshold were chosen and reflect tail probabilities of 0.001 and 0.05, respectively. In the temporary modeling case, the memory factor was reduced to 0.85, to reduce the weight on older estimates and increase the responsiveness to detecting the end of the fault. To this effect, "on" and "off" thresholds of 40 and 24 were chosen, reflecting tail probabilities of approximately 0.005 and 0.45 in a 20-degree-of-freedom chi-squared distribution.

For the MMAE SVSF-KF, initial filter probabilities were set at 0.95 for the KF and 0.05 for the SVSF. The likelihood function (22) was only computed for the position state, as from initial testing seemed to be the best indicator of fault. For the temporary modeling change case, an artificial lower bound on the KF probability estimate was set at 0.01, with a reset counter of 30 timesteps.

As for the IMM SVSF-KF, initial mode probabilities were set to 0.95 and 0.05 for the KF and SVSF, respectively. In addition, the likelihood function (30) was only used with respect to the position state to avoid numerical stability issues. The Markov transition probability matrix was defined as follows:

$$p = \begin{bmatrix} 0.99 & 0.01 \\ 0.01 & 0.99 \end{bmatrix}. \tag{45}$$

For our benchmark comparison, we shall use three test cases.

1) *Case One:* Permanent modeling change. The system suddenly switches from model $\boldsymbol{A_1}$ to $\boldsymbol{A_2}$ after 0.5 s. All filter models continue to use the incorrect $\boldsymbol{A_1}$ model.
2) *Case Two:* Temporary modeling change. The system suddenly switches from model $\boldsymbol{A_1}$ to $\boldsymbol{A_2}$ after 0.25 s and then back to $\boldsymbol{A_1}$ at 0.75 s. In this case, the filter's internal model will only be correct prior to 0.25 s and after 0.75 s.
3) *Case Three:* Permanent modeling change with step input. The system suddenly switches from model $\boldsymbol{A_1}$ to $\boldsymbol{A_2}$ after 0.5 s. At the same time, the system receives a large step input, onto which the original random input signal is superimposed. This serves to exacerbate the effect of the modeling error.

These test cases are used to evaluate the filter performance based on the following four metrics: the total root mean square error (RMSE) for each state estimate, the prefault RMSE, the fault RMSE, and the postfault RMSE for the case of temporary modeling change.

V. Results and Discussion

A. Case One: Permanent System Change

In this section, we describe the results of the simulations where a permanent system change is induced halfway through the simulation. The estimation performance of the KF and SVSF filters across all three states can be seen in Fig. 3. From this figure, it can be clearly seen that the position estimate of the KF begins to diverge from the measured state soon after the system change occurs at 0.5 s. In contrast, it is also apparent

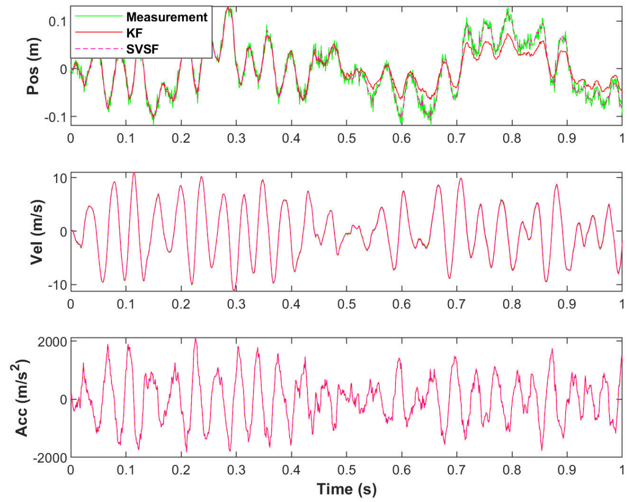

Fig. 3. Measured and estimated states from the KF and SVSF-KF in case one.

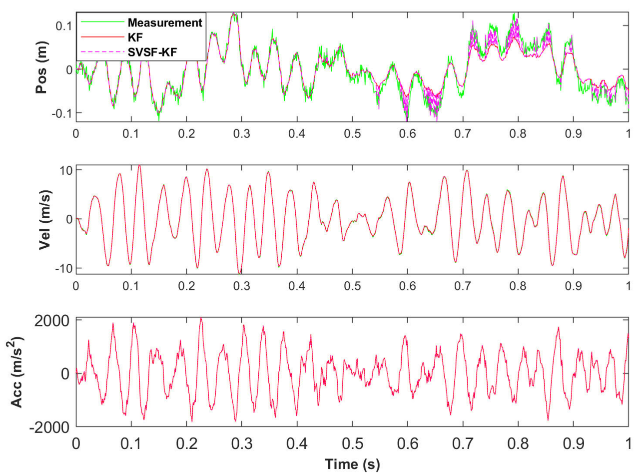

Fig. 4. Measured and estimated state from the KF and VBL-based SVSF-KF in case one.

from Fig. 3 that the SVSF's estimates are robust to the system change and exhibit superior performance in estimating the true state in comparison to the KF. Otherwise, the velocity and acceleration states do not convey any qualitative information about the filters' performances.

In Fig. 4, the estimates determined by the VBL-based SVSF-KF are shown alongside the KF estimates and measured states. It can be easily observed from this figure that the SVSF-KF faces difficulty in maintaining a stable estimate of the position upon the introduction of a fault or system change. Regardless of this observed chattering behavior, it is clear to see that the SVSF-KF is still more robust in detecting faults upon their occurrence. Upon closer look at the VBL's width and gain activation plot in Fig. 5, the reason behind this chattering effect is revealed. Despite the VBL's ability to readily detect the system change and grow beyond the set threshold, the frequent dropping of the VBL after each gain switch further aggravates a high-frequency switching between the two gains. As a result of this high-frequency switching, the overall effect is a degradation in estimation performance.

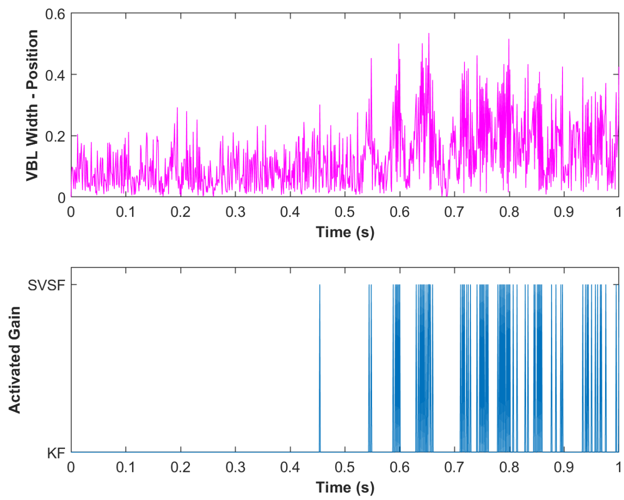

Fig. 5. VBL width for the position state (top) and gain activation plot (bottom) in case one.

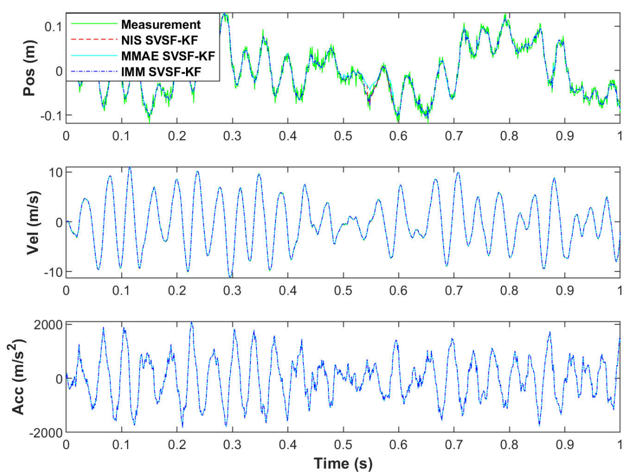

Fig. 6. Measured and estimated states from the three newly proposed SVSF-KF methods in case one.

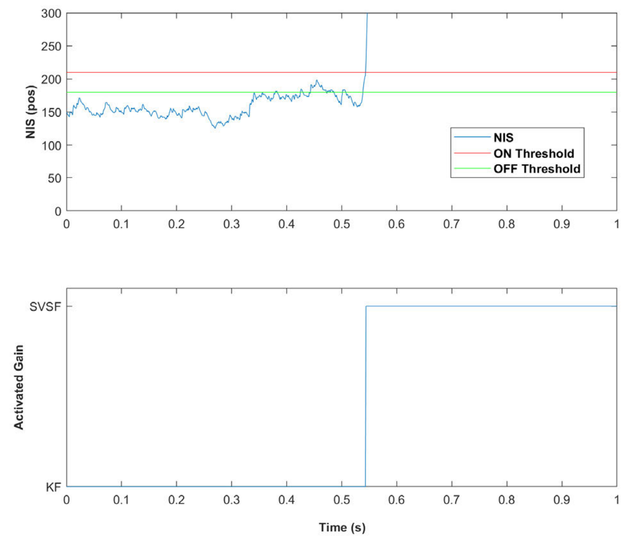

Fig. 7. NIS of estimated position state (top) and gain activation plot (bottom) in case one.

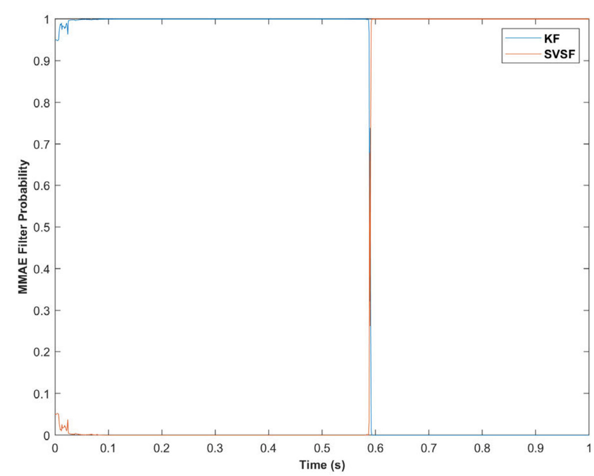

Fig. 8. Internal filter probabilities of the MMAE SVSF-KF in case one.

The three newly proposed SVSF-KF estimates are plotted in Fig. 6. From this figure, it is evident that all three filters provide a relatively robust estimate of the true state as inferred from the fact that they are hardly distinguishable from one another. Examining the NIS SVSF-KF's performance further, the NIS of its position estimate and corresponding gain activation plot is plotted in Fig. 7. As can be seen in the figure, the NIS appears to be able to detect the presence of the fault and grow beyond the switching threshold after the 0.5-s mark. Furthermore, the NIS SVSF-KF's switching gain is able to immediately activate and steadily maintain steady operation of the SVSF. As a result, the chattering effects previously observed from the VBL-based SVSF-KF are minimized if not eliminated, mainly thanks to the fact that the high-frequency switching behavior to and back from the KF is no longer present. A limitation that can be observed, however, is the fact that the switching to the SVSF is slightly delayed from the actual presence of the fault by approximately 40 ms.

In terms of the MMAE SVSF-KF, the probability of each filter being activated is plotted in Fig. 8. The MMAE SVSF-KF is shown to be able to accurately determine that the KF is the favorable filter prior to the occurrence of a fault. Furthermore, from the figure, it is shown that the filter is able to detect the fault, and in turn favor and switch to the SVSF. Similar to the NIS approach, the MMAE approach is able to maintain steady operation of the SVSF without any frequent switching to the KF whatsoever. One drawback of the MMAE approach, however, is that it is slower in reacting to the fault, requiring approximately 90 ms and subsequently rendering it slightly more than two times slower than the NIS approach.

The mode probabilities of the third and final model, the IMM SVSF-KF, are shown in Fig. 9. While the mode probabilities determined by the IMM method may seem noisy, they are generally able to correctly weigh the KF and SVSF for prior to and after the fault, respectively. However, from the figure, the IMM approach tends to display jerky behavior at certain points of the simulation quite often. This can be observed by the less optimal filter for the normal or faulty condition, i.e., the SVSF and KF, respectively, is triggered momentarily. Otherwise, the

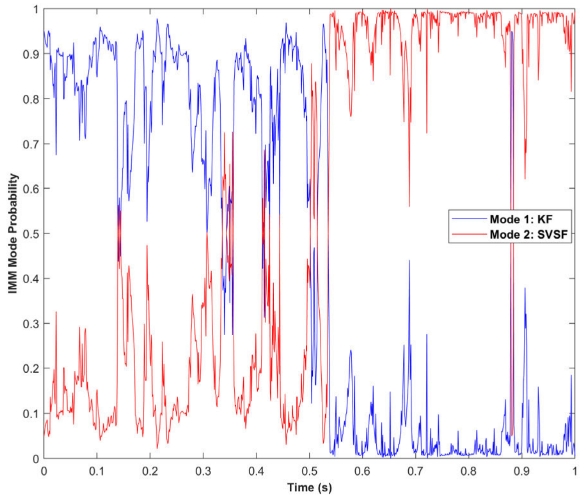

Fig. 9. Internal filter probabilities of the IMM SVSF-KF in case one.

TABLE II
RMSE Results of Filters Under Case One Conditions

		KF	SVSF	SVSF-KF	NIS SVSF-KF	MMAE SVSF-KF	IMM SVSF-KF
Pre-fault	*Pos*	0.0030	0.0047	0.0031	0.0030	0.0030	0.0032
	Vel	0.0388	0.0469	0.0388	0.0388	0.0388	0.0393
	Acc	0.7352	0.9779	0.7360	0.7352	0.7354	0.7506
Fault	*Pos*	0.0174	0.0047	0.0146	0.0051	0.0057	0.0048
	Vel	0.0934	0.0473	0.0834	0.0480	0.0499	0.0466
	Acc	0.9039	0.8637	0.9301	0.8475	0.8464	0.8341
Total	*Pos*	0.0152	0.0060	0.0131	0.0054	0.0061	0.0052
	Vel	0.0879	0.0600	0.0796	0.0552	0.0567	0.0544
	Acc	1.0307	1.1525	1.0525	0.9975	0.9968	0.9968

IMM SVSF-KF is able to detect and react to the change in roughly the same time as the NIS SVSF-KF.

A Monte Carlo simulation was carried out with 500 runs, and the quantitative results from this simulation are presented in Table II, whereby the RMSE value for each estimated state is shown, and each filter's performance is broken down into prefault, postfault, and total RMSE values. A color-coded heatmap based on the percentile of the results is implemented in the table to simplify the analysis of the results. Specifically, the highest performances (90th percentile) are shaded in green, followed by a shade of yellow for mid-tier performance (50th percentile), and finally by a shadow of red for the worst performance (tenth percentile). The units for the position, velocity, and acceleration errors are m, (m/s), and (m/s^2), respectively.

Several observations and inferences can be made regarding the performance of each filter upon examination of Table II. First, it can be observed that the KF displays the lowest error in the prefault stage of the simulation for all three states, tied with the NIS SVSF-KF. This superior performance does not extend into the faulty stage of the simulation, which clearly shows the KF estimate errors deteriorating, ultimately resulting in one of the lowest total RMSE scores of all the filters. As for the SVSF, poor performance is demonstrated in the prefault stage, with significantly improved performance during the fault stage. However, the total of the RMSE of the SVSF is still within the lowest quintile. As for the SVSF-KF, average performance is apparent in the prefault stage compared to the KF, with the same poor performance during the system change and overall.

When examining the RMSE of all three newly proposed SVSF-KF approaches, a clear improvement in performance can be seen across all stages of the simulation when compared to the KF, SVSF, and SVSF-KF. Overall, it can be argued that the NIS SVSF-KF demonstrates the best performance across all stages of the simulation. The MMAE SVSF-KF shows slight degradation in performance when the fault is introduced, but still maintains low total RMSE values. As for the IMM SVSF-KF, it demonstrates the best performance in the presence of a fault, but at the cost of degradation in performance prior to the fault. By taking the average total RMSE across all three states for the filters, the NIS SVSF-KF represents an improvement of 19% in average total RMSE compared to the worst-performing filter, the KF. Compared to the SVSF-KF, the NIS-SVSF-KF represents an 8% improvement in average total RMSE.

B. Case Two: Temporary Fault Condition

In the second case of experimental simulations, the EHA suddenly switches to the alternate faulty system at t = 0.25 s, and switches back at t = 0.75 s to the normal system conditions. This test is more difficult as it requires each filter to detect the onset of the system change, as well as its conclusion. The state estimates for this scenario determined by the general KF and SVSF are plotted in Fig. 10. From the figure, similar observations can be made to the previous case, in that the KF begins to exhibit noticeable divergence in its position state estimate upon the introduction of the fault at 0.25 s. The KF is able to recover upon the conclusion of faulty conditions to yield an accurate estimate. As for the SVSF, it can be seen to present robust estimation performance even during the presence of fault, and throughout the entire simulation.

The state estimates from the VBL-based SVSF-KF are presented in Fig. 11. In the figure, specifically from the estimate of the position state, it is clear that the SVSF-KF can detect the fault rather quickly and attempt to adapt. Similarly, the conclusion of the fault is also detected, and the filter is able to revert back to its original operation. However, as in the previous case, the SVSF-KF begins to display some chattering when it attempts to account for and act in the presence of the system fault. Otherwise, no observable difference in performance is visible in the estimates of the velocity and acceleration states between the two filters. By inspecting Fig. 12, the cause of the chattering in the SVSF-KF estimate can be attributed to the same high-frequency switching behavior of the activation gain during the presence of the fault. Regardless, it is also clear from Fig. 12 that the SVSF-KF can instantaneously detect the presence and subsequent absence of the fault with no delay.

The three new SVSF-KF formulations and their state estimates are shown in Fig. 13. In this figure, all three of the approaches display robust performance throughout the entire simulation, despite the presence of the temporary fault. In fact, other than a slight deviation by the MMAE SVSF-KF at the

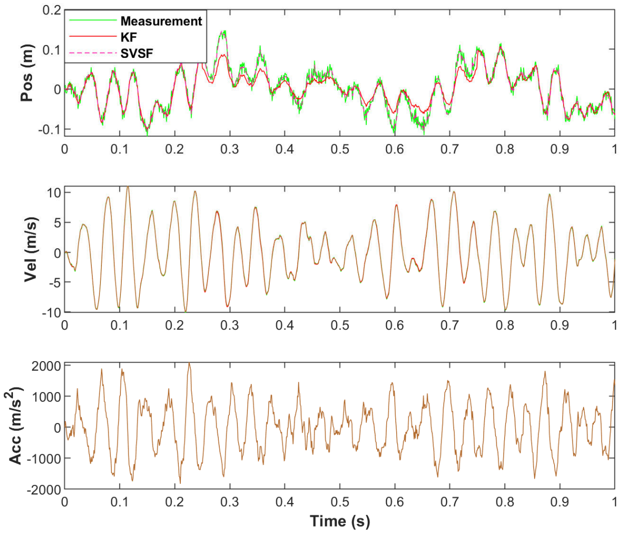

Fig. 10. Measured and estimated states from the KF and SVSF-KF in case two.

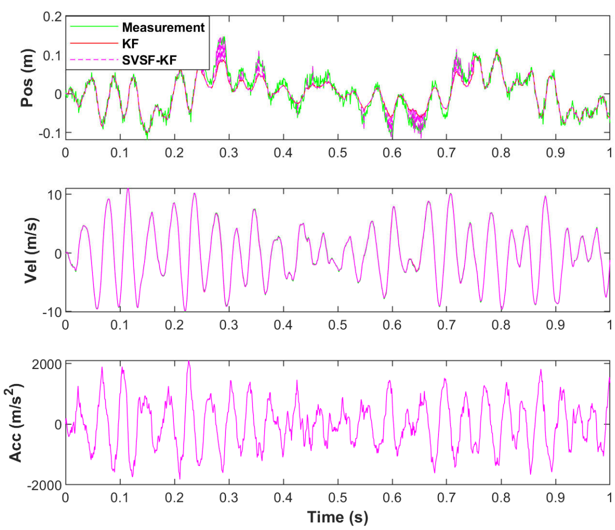

Fig. 11. Measured and estimated state from the KF and VBL-based SVSF-KF in case two.

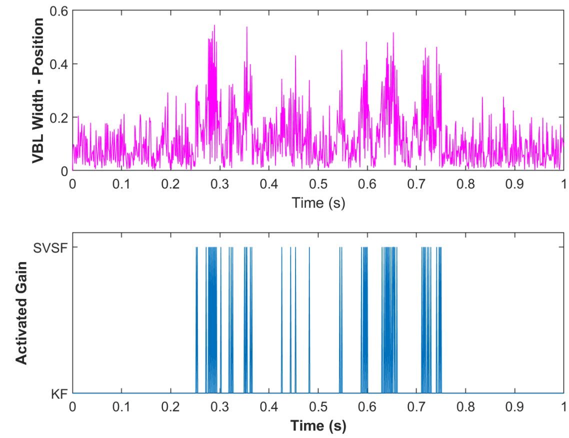

Fig. 12. VBL width for the position state (top) and gain activation plot (bottom) in case two.

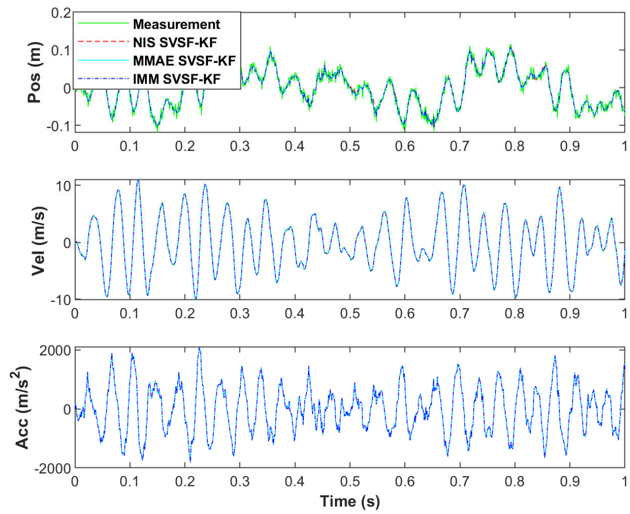

Fig. 13. Measured and estimated states from the three newly proposed SVSF-KF methods in case two.

moment the fault is introduced at 0.25 s, the performances of all three filters can barely be distinguishable from one another and all are able to maintain accurate estimates with no sign of divergence, unlike with the previous KF simulation.

Fig. 14 shows a plot of the NIS of the position estimate as well as a plot of the NIS SVSF-KF activation gain. Within these plots, it is evident that the NIS SVSF-KF is able to instantaneously identify the presence of the fault without delay, and steadily maintain its gain activation accordingly for most of the fault's duration. Similarly, the NIS SVSF-KF is shown to detect the passing of the fault, with a short delay of approximately between 10 and 15 ms. However, the NIS SVSF-KF does exhibit brief drops in the activation gain halfway through the fault's duration. As a result, there is a temporary switch to the KF gain instead of the more robust SVSF. This particular behavior is not considered desirable, and deemed by the authors to be possibly a result of improper tuning of the fading memory parameter α. Thus, further improvements in performance may be realized by improved tuning practices and even possibly by adjustments to the switching thresholds. The NIS SVSF-KF still, however, exhibits overall consistent use of the SVSF gain appropriately and without the high-frequency switching exhibited by the VBL-based SVSF-KF.

The plots of the MMAE and IMM internal filter mode probabilities are shown in Figs. 15 and 16, respectively. From these two figures, it is clear that both the MMAE and IMM SVSF-KF are able to instantaneously detect the presence of the system fault and adjust accordingly. However, when the fault is no longer present, the MMAE SVSF-KF is not able to respond and switch back to the KF gain as rapidly as the IMM SVSF-KF or the NISSVSF-KF. Overall, the NIS approach had the fastest reaction of approximately 10–15 ms, then the IMM SVSF-KF with a reaction of 20 ms, and finally the MMAE SVSF-KF with a reaction time of 50 ms. It is worth noting that despite its other limitations, the SVSF-KF is fastest in reacting to the passing of the fault, doing so instantaneously.

The RMSE results of each of the studied filters are presented in Table III. As in the first simulation case, the RMSE results

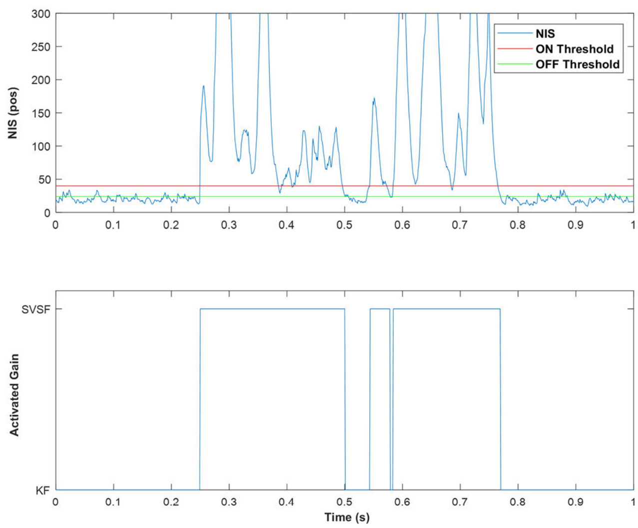

Fig. 14. NIS of estimated position state (top) and gain activation plot (bottom) in case two.

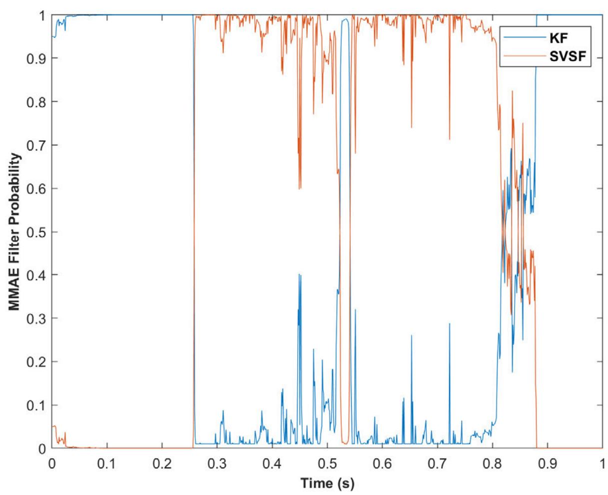

Fig. 15. Internal filter model probabilities of the MMAE SVSF-KF in case two.

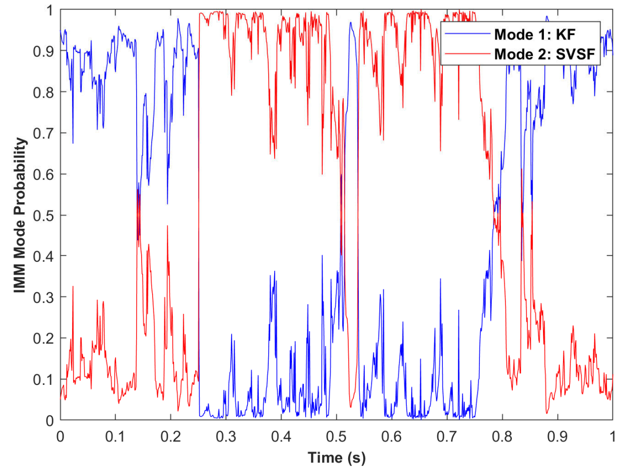

Fig. 16. Internal filter mode probabilities of the IMM SVSF-KF in case two.

TABLE III
RMSE Results of Filters Under Case Two Conditions

		KF	SVSF	SVSF-KF	NIS SVSF-KF	MMAE SVSF-KF	IMM SVSF-KF
Pre - fault	*Pos*	0.0094	0.0047	0.0082	0.0041	0.0044	0.0040
	Vel	0.0623	0.0470	0.0581	0.0432	0.0461	0.0429
	Acc	0.8054	0.9235	0.8176	0.7939	1.6108	0.8001
Fault	*Pos*	0.0167	0.0047	0.0141	0.0052	0.0049	0.0048
	Vel	0.0900	0.0475	0.0809	0.0482	0.0516	0.0468
	Acc	0.8939	0.8650	0.9198	0.8485	3.0676	0.8406
Post - fault	*Pos*	0.0032	0.0047	0.0032	0.0032	0.0034	0.0033
	Vel	0.0394	0.0471	0.0394	0.0397	0.0404	0.0401
	Acc	0.7497	0.9816	0.7451	0.7596	0.8413	0.7737
Total	*Pos*	0.0145	0.0060	0.0125	0.0054	0.0059	0.0053
	Vel	0.0848	0.0600	0.0770	0.0554	0.0591	0.0547
	Acc	1.0276	1.1556	1.0451	1.0065	3.1980	1.0127

are tabulated for each of the three states during the prefault, fault, and postfault stages. It can be seen from this table that the KF, unlike in the previous simulations, does not exhibit superior performance in the prefault stages, and instead the NIS SVSF-KF and IMM SVSF-KF exhibit the best prefault RMSE values. When the fault is introduced, the SVSF is shown to have the lowest and most favorable RMSE values, followed closely by the IMM SVSF-KF and NIS SVSF-KF. However, this superior performance does not warrant the SVSF favorable as its state estimates in the prefault and postfault stages are in the lowest percentile across all filters. A similar trend is apparent with the SVSF-KF, except that the superior performance is exhibited in the postfault, and not the prefault and fault stages. Overall, the original KF, SVSF, and VBL-based SVSF-KF demonstrate some of the lowest RMSE values when compared to the three newer SVSF-KF strategies.

Of the three newly proposed SVSF-KF strategies, as previously mentioned, the NIS SVSF-KF and IMM SVSF-KF exhibit the lowest RMSE values during the prefault stage. Furthermore, these two methods also result in the two lowest total RMSE values in the overall simulation. Upon the occurrence of the fault, the IMM SVSF-KF's performance is slightly more favorable than the NIS SVSF-KF by an average RMSE of just 1%. In the postfault stage, the NIS-SVSF-KF shows superior performance than the IMM SVSF-KF. As for the MMAE SVSF-KF, its performance across all stages of the simulation is inferior to that of its NIS and IMM counterparts. Thus, it can be concluded that the NIS SVSF-KF once more demonstrates the most effective estimation performance across all filters studied. The NIS represents an average total RMSE improvement of 6% over the SVSF-KF and less than 1% than the IMM SVSF-KF.

C. Case Three: Temporary Fault With Concurrent Step Input

In the third simulation scenario, the conditions are almost identical to that of the first case, except for one slight difference. In this experiment, a unit step input is superimposed onto the original input signal at the time the system uncertainty is introduced halfway through the simulation. The purpose of doing so is to exacerbate the effect of the system uncertainty

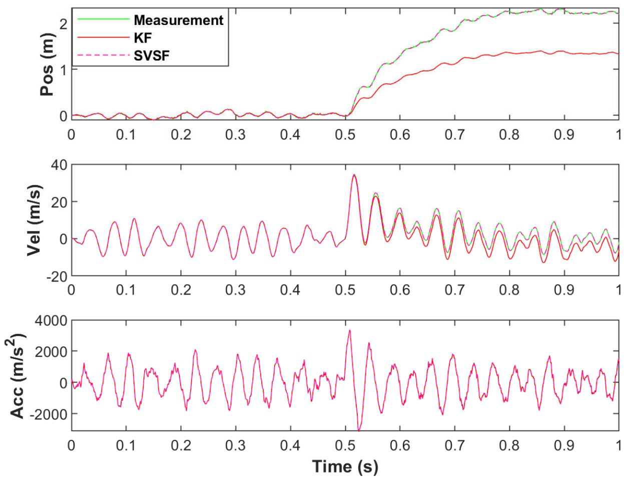

Fig. 17. Measured and estimated states from the KF and SVSF-KF in case three.

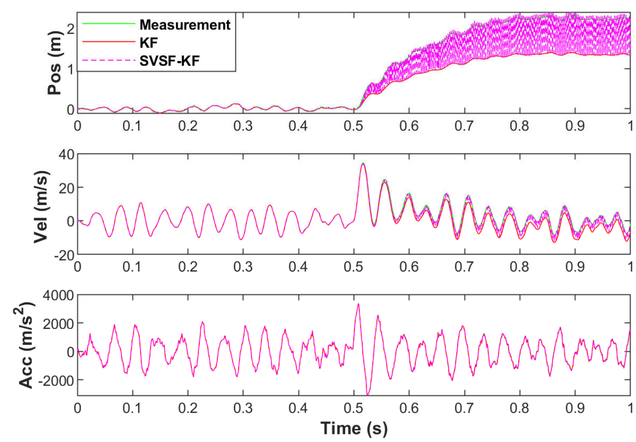

Fig. 18. Measured and estimated state from the KF and VBL-based SVSF-KF in case three.

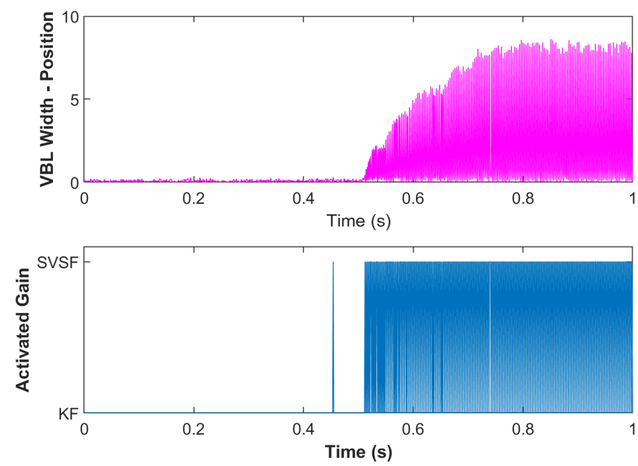

Fig. 19. VBL width for the position state (top) and gain activation plot (bottom) in case three.

and observe the resultant effect on the performance of the different filters.

In Fig. 17, the KF performs poorly when faced with the structural uncertainty and unit step input at 0.5 s. In fact, the KF performs significantly worse than the two previously studied cases when observing the position state estimate. As such, it can be inferred that the KF's performance degradation is exacerbated by the severity of the uncertainty encountered. The SVSF, in contrast, manages to maintain a relatively accurate estimate across all three states. It is interesting to observe that in this scenario, the KF's velocity estimate begins to diverge from the measured state. This is an event that has not occurred in the previous two cases studied and further supports the inferences regarding the KF's worsening performance in the face of increasingly severe faults.

The VBL-based SVSF-KF state estimates are plotted in Fig. 18, which demonstrate the same chattering behavior in the position state as in the previous two cases. This deterioration in the state estimate is confirmed to be a result of the high-frequency switching commonly experienced by the VBL-based approach, as can be seen in the plot of the gain activation in Fig. 19. In this case, the degradation of performance is further exacerbated by the unit step input, which results in the increased amount of chattering observed from Fig. 18.

The estimates of the three newly proposed SVSF-KF approaches under the step input conditions are plotted in Fig. 20. It is clear from this figure that all three newly proposed methods are able to robustly deal with the structural uncertainty despite being exacerbated further by a unit step input. In fact, there is no divergence visible by either the NIS, MMAE, or IMM SVSF-KF when qualitatively examining all three state estimates from Fig. 20. Upon further examination of the activation gain of the NIS shown in Fig. 21, it can be seen that it is capable of detecting the fault and switching to the SVSF within 10 ms of its occurrence in a steady and stable fashion. This also holds true for both the MMAE and IMM approaches, as seen in Figs. 22 and 23, respectively, which both manage to detect the fault in the same amount of time. Surprisingly, both approaches seem to display steady maintenance of the SVSF mode without any of the exuberant characteristics observed in previous cases. Furthermore, it is also interesting to note that IMM SVSF-KF exhibits more stable switching behavior during the exacerbated fault than it does prior to the fault's occurrence. A possible inference can be made that the IMM approach may perform better in more severe circumstances and scenarios.

The RMSE results of the third case are presented in the estimates of the three newly proposed SVSF-KF approaches under the step input conditions are plotted in Fig. 20. It is clear from this figure that all three newly proposed methods are able to robustly deal with the structural uncertainty despite being exacerbated further by a unit step input. In fact, there is no divergence visible by either the NIS, MMAE, or IMM SVSF-KF when qualitatively examining all three state estimates from Fig. 20. Upon further examination of the activation gain of the NIS shown in Fig. 21, it can be seen that it is capable of detecting the fault and switching to the SVSF within 10 ms of its occurrence in a steady and stable fashion. This also holds true for both the MMAE and IMM approaches, as seen in Figs. 22 and 23, respectively, which both manage to detect the fault in the same amount of time. Surprisingly, both

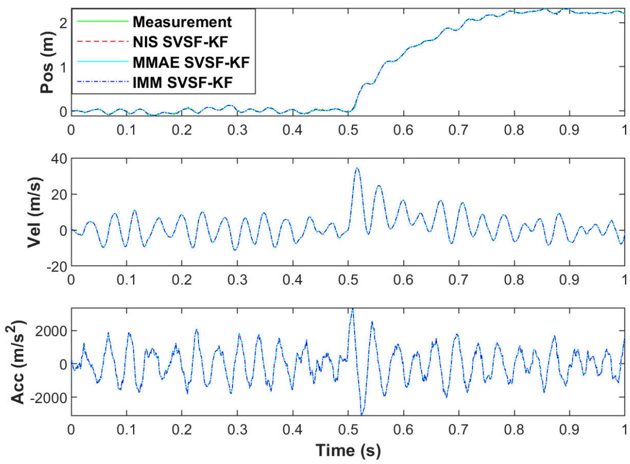

Fig. 20. Measured and estimated states from the three newly proposed SVSF-KF methods in case three.

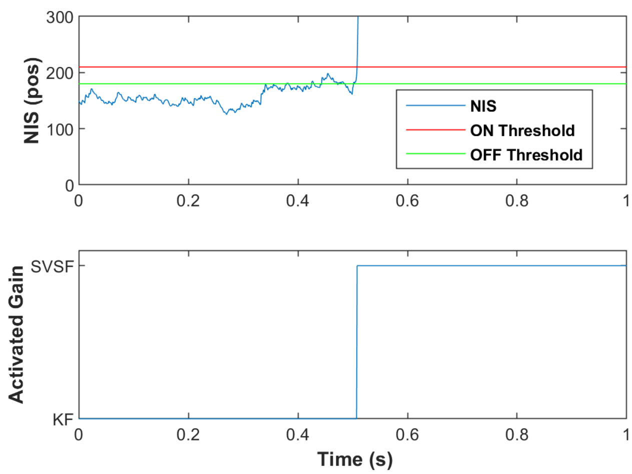

Fig. 21. NIS of estimated position state (top) and gain activation plot (bottom) in case three.

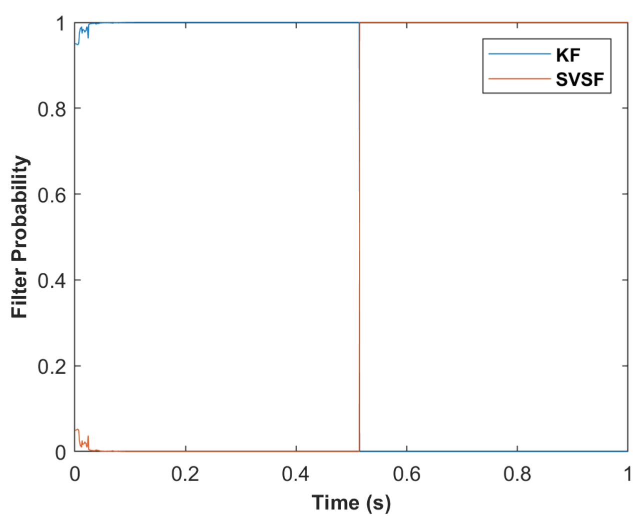

Fig. 22. Internal filter model probabilities of the MMAE SVSF-KF in case three.

approaches seem to display steady maintenance of the SVSF mode without any of the exuberant characteristics observed in previous cases. Furthermore, it is also interesting to note that IMM SVSF-KF exhibits more stable switching behavior during the exacerbated fault than it does prior to the fault's occurrence. A possible inference can be made that the IMM approach may perform better in more severe circumstances and scenarios.

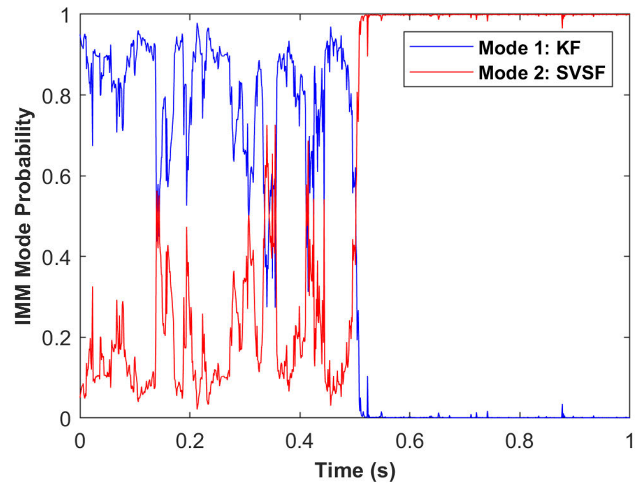

Fig. 23. Internal filter mode probabilities of the IMM SVSF-KF in case three.

TABLE IV
RMSE Results of Filters Under Case Three Conditions

		KF	SVSF	SVSF-KF	NIS SVSF-KF	MMAE SVSF-KF	IMM SVSF-KF
Pre-fault	*Pos*	0.0030	0.0047	0.0031	0.0030	0.0030	0.0032
	Vel	0.0388	0.0469	0.0388	0.0388	0.0388	0.0393
	Acc	0.7352	0.9779	0.7360	0.7352	0.7354	0.7506
Fault	*Pos*	0.7055	0.0047	0.2650	0.0048	0.0054	0.0050
	Vel	3.5475	0.0473	1.0599	0.0477	0.0503	0.0485
	Acc	20.8860	0.8023	9.2761	0.8035	0.8304	0.8033
Total	*Pos*	0.5270	0.0060	0.3063	0.0052	0.0068	0.0059
	Vel	2.6497	0.0600	1.1991	0.0550	0.0595	0.0573
	Acc	15.5445	1.1148	10.5281	0.9658	0.9962	0.9754

Table IV, following the same procedures previously discussed to color the results based on a heatmap of performance percentiles. As expected, the KF performs well only during the prefault stages, with performance comparable to that of the NIS SVSF-KF in the same stage. In the fault stage, this performance does not last and instead, the KF fails to perform as well as other filters, as expected. The SVSF displays the opposite performance than the KF, performing poorly prior to the fault, and exceptionally well during the fault. As for the SVSF-KF, it displays effective performance in the prefault stage but does not perform as well as the SVSF during the presence of the fault. Similar to the previous cases and as would be expected at this point of the analysis, the three newly proposed SVSF-KF methods exhibit the lowest RMSE values of all the filters studied. Overall, however, it is the NIS SVSF-KF that shows the best performance across all states and operating stages. The improvement of the average total RMSE value of NIS SVSF-KF over the SVSF-KF and IMM SVSF-KF is 92% and 1.5%, respectively.

VI. Conclusion

The SVSF-KF is an adaptive estimation strategy that provides an optimal KF estimate during normal system operation, and a robust SVSF estimate in faulty conditions. However, the SVSF-KF has been shown to have limitations in its performance, largely due to the VBL-based gain adaptation method used to switch between the two filters. In response, this article presents three new approaches, termed the NIS SVSF-KF, MMAE SVSF-KF, and IMM SVSF-KF, with the goal of addressing the issues encountered by the VBL-based gain adaptation. An experimental simulation is conducted to observe the estimation performance of the three newly proposed approaches in comparison to the KF, SVSF, and VBL-based SVSF-KF. The simulations involve an electro hydrostatic actuator test case which is subject to a fault at certain points of the simulation.

The newly proposed SVSF-KF approaches have been proven to outperform the original VBL-based SVSF-KF approach, as well as the original standalone KF and SVSF. Namely, it was shown that the proposed NIS SVSF-KF can address and minimize the effects of chattering generally observed by the VBL SVSF-KF. Furthermore, we demonstrated that the NIS SVSF-KF exhibits the best overall performance in estimating the states of the EHA under faulty conditions, followed by the MMAE and IMM SVSF-KF. Despite these results, however, each of the newly proposed methods was associated with its own advantages and limitations. The NIS approach, for example, requires careful tuning and selection of the fading memory parameter, as well as the switching thresholds. In this respect, depending on the circumstances and application, the IMM approach may be a more suitable choice in more stringent cases. Another main limitation of both the IMM and MMAE approaches is the fact that a combined weighting of the SVSF and KF estimates was often used when it was optimally desired to have just one or the other.

Future study will involve investigating modification of the MMAE and IMM approaches, forcing them to apply full weight to the filter or mode identified to be the most likely mode, instead of allowing for a combined weighting scheme. Furthermore, future studies will also include a full exposition of the performance of the proposed strategies with other popular adaptive estimation strategies found the in literature. This comparative study will consider aspects such as convergence speed, computational complexity, accuracy, and performance, as well as a full investigation into the effects related to parameter uncertainties through a thorough sensitivity analysis study.

References

[1] R. E. Kalman, "A new approach to linear filtering and prediction problems," *J. Basic Eng.*, vol. 82, no. 1, pp. 35–45, Mar. 1960, doi: 10.1115/1.3662552.

[2] M. S. Grewal and A. P. Andrews, *Kalman Filtering: Theory and Practice With MATLAB*, vol. 9781118851210, 4th ed. Hoboken, NJ, USA: Wiley, 2014, doi: 10.1002/9781118984987.

[3] H. Zhao and Z. Wang, "Motion measurement using inertial sensors, ultrasonic sensors, and magnetometers with extended Kalman filter for data fusion," *IEEE Sensors J.*, vol. 12, no. 5, pp. 943–953, May 2012, doi: 10.1109/JSEN.2011.2166066.

[4] X. Liu et al., "Kalman filter-based data fusion of Wi-Fi RTT and PDR for indoor localization," *IEEE Sensors J.*, vol. 21, no. 6, pp. 8479–8490, Mar. 2021, doi: 10.1109/JSEN.2021.3050456.

[5] M. Arsalan, A. Santra, and C. Will, "Improved contactless heartbeat estimation in FMCW radar via Kalman filter tracking," *IEEE Sensors Lett.*, vol. 4, no. 5, pp. 1–4, May 2020, doi: 10.1109/LSENS.2020.2983706.

[6] A. Gelb, *Applied Optimal Estimation*, vol. 64, no. 4. Cambridge MA, USA: MIT Press, 2001.

[7] R. G. Brown and P. Y. C. Hwang, *Introduction to Random Signals and Applied Kalman Filtering*, no. 4. Hoboken, NJ, USA: Wiley, 1997.

[8] P. S. Maybeck, "Stochastic models, estimation, and control—Introduction," in *Stochastic Models, Estimation, and Control*. New York, NY, USA: Academic, 1979.

[9] H. H. Afshari, S. A. Gadsden, and S. Habibi, "Gaussian filters for parameter and state estimation: A general review of theory and recent trends," *Signal Process.*, vol. 135, pp. 218–238, Jun. 2017, doi: 10.1016/j.sigpro.2017.01.001.

[10] H. Zhou, L. Xu, W. Chen, K. Guo, F. Shen, and Z. Guo, "A novel robust filtering strategy for systems with non-Gaussian noises," *AEU Int. J. Electron. Commun.*, vol. 97, pp. 154–164, Dec. 2018, doi: 10.1016/j.aeue.2018.10.004.

[11] S. Mahfouz, F. Mourad-Chehade, P. Honeine, J. Farah, and H. Snoussi, "Target tracking using machine learning and Kalman filter in wireless sensor networks," *IEEE Sensors J.*, vol. 14, no. 10, pp. 3715–3725, Oct. 2014, doi: 10.1109/JSEN.2014.2332098.

[12] A. Assa and F. Janabi-Sharifi, "A Kalman filter-based framework for enhanced sensor fusion," *IEEE Sensors J.*, vol. 15, no. 6, pp. 3281–3292, Jun. 2015, doi: 10.1109/JSEN.2014.2388153.

[13] F. L. Lewis, L. Xie, and D. Popa, *Optimal and Robust Estimation: With an Introduction to Stochastic Control Theory*, 2nd ed. Boca Raton, FL, USA: CRC Press, 2007.

[14] U. Shaked and Y. Theodor, "H_∞-optimal estimation: A tutorial," in *Proc. 31st 31st IEEE Conf. Decision Control*, Dec. 1992, pp. 2278–2286.

[15] D. Simon, *Optimal State Estimation: Kalman, H_∞, and Nonlinear Approaches*. Hoboken, NJ, USA: Wiley, 2006, doi: 10.1002/0470045345.

[16] Y. Shtessel, C. Edwards, L. Fridman, and A. Levant, *Sliding Mode Control and Observation*. New York, NY, USA: Birkhäuser, 2014, doi: 10.1007/978-0-8176-4893-0.

[17] S. R. Habibi and R. Burton, "The variable structure filter," *J. Dyn. Syst., Meas., Control*, vol. 125, no. 3, pp. 287–293, Sep. 2003, doi: 10.1115/1.1590682.

[18] S. Habibi, "The smooth variable structure filter," *Proc. IEEE*, vol. 95, no. 5, pp. 1026–1059, May 2007, doi: 10.1109/JPROC.2007.893255.

[19] Y. Bar-Shalom, X.-R. Li, and T. Kirubarajan, *Estimation With Applications to Tracking and Navigation*. Hoboken, NJ, USA: Wiley, 2001, doi: 10.1002/0471221279.

[20] H. Musoff and P. Zarchan, *Fundamentals of Kalman Filtering: A Practical Approach*, 3rd ed. Reston, VA, USA: American Institute of Aeronautics and Astronautics, 2009, doi: 10.2514/4.867200.

[21] M. Spiller and D. Söffker, "On the relation between smooth variable structure and adaptive Kalman filter," *Frontiers Appl. Math. Statist.*, vol. 6, pp. 1–3, Nov. 2020, doi: 10.3389/fams.2020.585439.

[22] A. Šabanovic, "Variable structure systems with sliding modes in motion control—A survey," *IEEE Trans. Ind. Informat.*, vol. 7, no. 2, pp. 212–223, May 2011, doi: 10.1109/TII.2011.2123907.

[23] V. Utkin, "Variable structure systems with sliding modes," *IEEE Trans. Autom. Control*, vol. AC-22, no. 2, pp. 212–222, Apr. 1977, doi: 10.1109/TAC.1977.1101446.

[24] M. Avzayesh, M. Abdel-Hafez, M. AlShabi, and S. A. Gadsden, "The smooth variable structure filter: A comprehensive review," *Digit. Signal Process.*, vol. 110, Mar. 2021, Art. no. 102912, doi: 10.1016/j.dsp.2020.102912.

[25] S. A. Gadsden and M. Al-Shabi, "A study of variable structure and sliding mode filters for robust estimation of mechatronic systems," in *Proc. IEEE Int. IoT, Electron. Mechatronics Conf. (IEMTRONICS)*, Sep. 2020, pp. 1–6, doi: 10.1109/iemtronics51293.2020.9216381.

[26] H. Afshari, D. Al-Ani, and S. Habibi, "State estimation of a faulty actuator using the second-order smooth variable structure filter (the 2ND-order SVSF)," in *Proc. IEEE 28th Can. Conf. Electr. Comput. Eng. (CCECE)*, May 2015, pp. 919–924, doi: 10.1109/CCECE.2015.7129398.

[27] H. H. Afshari, S. A. Gadsden, and S. R. Habibi, "Robust fault diagnosis of an electro-hydrostatic actuator using the novel dynamic second-order SVSF and IMM strategy," *Int. J. Fluid Power*, vol. 15, no. 3, pp. 181–196, 2014, doi: 10.1080/14399776.2014.981134.

[28] S. Gadsden, "Smooth variable structure filtering: Theory and applications," Ph.D. thesis, McMaster Univ., Hamilton, ON, Canada, Tech. Rep., 2011. [Online]. Available: http://hdl.handle.net/11375/11249

[29] M. Al-Shabi, "The general toeplitz/observability SVSF," Ph.D. thesis, McMaster Univ., Hamilton, ON, Canada, Tech. Rep., 2011. [Online]. Available: http://hdl.handle.net/11375/21180

[30] H. Suwoyo et al., "Maximum likelihood estimation-assisted ASVSF through state covariance-based 2D SLAM algorithm," *TELKOMNIKA (Telecommun. Comput. Electron. Control)*, vol. 19, no. 1, p. 327, Feb. 2021, doi: 10.12928/telkomnika.v19i1.16223.

[31] M. Al-Shabi and S. Habibi, "New novel time-varying and robust smoothing boundary layer width for the smooth variable structure filter," in *Proc. 9th Int. Symp. Mechatronics Appl. (ISMA)*, Apr. 2013, pp. 1–6, doi: 10.1109/ISMA.2013.6547375.

[32] W. Li, H. Gu, and W. Su, "Partitioned time-varying smooth variable structure filter for airport target tracking," in *Proc. CIE Int. Conf. Radar (RADAR)*, Oct. 2016, pp. 1–5, doi: 10.1109/RADAR.2016.8059444.

[33] S. A. Gadsden, M. Al-Shabi, and T. Kirubarajan, "Square-root formulation of the SVSF with applications to nonlinear target tracking problems," *Proc. SPIE*, vol. 9474, May 2015, Art. no. 947408, doi: 10.1117/12.2177226.

[34] S. A. Gadsden and A. S. Lee, "Advances of the smooth variable structure filter: Square-root and two-pass formulations," *J. Appl. Remote Sens.*, vol. 11, no. 1, Mar. 2017, Art. no. 015018, doi: 10.1117/1.jrs.11.015018.

[35] H. Afshari, "The 2nd-order smooth variable structure filter (2nd-SVSF) for state estimation: Theory and applications," Ph.D. thesis, McMaster Univ., Hamilton, ON, Canada, Tech. Rep., 2015. [Online]. Available: http://hdl.handle.net/11375/16527

[36] H. H. Afshari, S. A. Gadsden, and S. Habibi, "Condition monitoring of an electro-hydrostatic actuator using the dynamic 2nd-order smooth variable structure filter," in *Proc. ASME/IEEE Int. Conf. Mech. Embedded Syst. Appl.*, vol. 9, Aug. 2015, pp. 1–6, doi: 10.1115/detc2015-47436.

[37] H. H. Afshari, S. A. Gadsden, and S. Habibi, "A nonlinear second-order filtering strategy for state estimation of uncertain systems," *Signal Process.*, vol. 155, pp. 182–192, Feb. 2019, doi: 10.1016/j.sigpro.2018.09.036.

[38] M. Attari, Z. Luo, and S. Habibi, "An SVSF-based generalized robust strategy for target tracking in clutter," *IEEE Trans. Intell. Transp. Syst.*, vol. 17, no. 5, pp. 1381–1392, May 2016, doi: 10.1109/TITS.2015.2504331.

[39] F. Demim, A. Nemra, and K. Louadj, "Robust SVSF-SLAM for unmanned vehicle in unknown environment," *IFAC-PapersOnLine*, vol. 49, no. 21, pp. 386–394, 2016, doi: 10.1016/j.ifacol.2016.10.585.

[40] S. A. Gadsden, M. Al-Shabi, and T. Kirubarajan, "Two-pass smoother based on the SVSF estimation strategy," *Proc. SPIE*, vol. 9474, May 2015, Art. no. 947409, doi: 10.1117/12.2177256.

[41] F. Demim, A. Nemra, K. Louadj, M. Hamerlain, and A. Bazoula, "Cooperative SLAM for multiple UGVs navigation using SVSF filter," *Automatika*, vol. 58, no. 1, pp. 119–129, Jan. 2017, doi: 10.1080/00051144.2017.1372123.

[42] F. Outamazirt, L. Yan, F. Li, and A. Nemra, "Comparing between the performance of SVSF with EKF and NH8 for the autonomous airborne navigation problem," in *Proc. IEEE Aerosp. Conf.*, Mar. 2016, pp. 1–8, doi: 10.1109/AERO.2016.7500504.

[43] J. Goodman, J. Kim, A. S. Lee, S. A. Gadsden, and M. Al-Shabi, "A variable structure-based estimation strategy applied to an RRR robot system," *J. Robot., Netw. Artif. Life*, vol. 4, no. 2, p. 142, 2017, doi: 10.2991/jrnal.2017.4.2.8.

[44] J. Goodman, J. Kim, A. S. Lee, S. A. Gadsden, and M. Al-Shabi, "Nonlinear estimation strategies applied on an RRR robotic manipulator," in *Proc. Int. Conf. Artif. Life Robot.*, vol. 22, 2017, pp. 342–345, doi: 10.5954/icarob.2017.gs9-5.

[45] F. Demim, A. Nemra, K. Louadj, M. Hamerlain, and A. Bazoula, "A new approach to improve the success and solving the UGVs cooperation for SLAM problem, using a SVSF filter," in *Proc. Medit. Conf. Pattern Recognit. Artif. Intell.*, Nov. 2016, pp. 56–63, doi: 10.1145/3038884.3038894.

[46] S. A. Gadsden and T. Kirubarajan, "Development of a variable structure-based fault detection and diagnosis strategy applied to an electromechanical system," *Proc. SPIE*, vol. 10200, pp. 422–435, May 2017, doi: 10.1117/12.2262570.

[47] W. Youn and S. A. Gadsden, "Combined quaternion-based error state Kalman filtering and smooth variable structure filtering for robust attitude estimation," *IEEE Access*, vol. 7, pp. 148989–149004, 2019, doi: 10.1109/ACCESS.2019.2946609.

[48] M. Attari, S. Habibi, and S. A. Gadsden, "Target tracking formulation of the SVSF with data association techniques," *IEEE Trans. Aerosp. Electron. Syst.*, vol. 53, no. 1, pp. 12–25, Feb. 2017, doi: 10.1109/TAES.2017.2649138.

[49] F. Outamazirt, L. Fu, Y. Lin, and N. Abdelkrim, "A new SINS/GPS sensor fusion scheme for UAV localization problem using nonlinear SVSF with covariance derivation and an adaptive boundary layer," *Chin. J. Aeronaut.*, vol. 29, no. 2, pp. 424–440, Apr. 2016, doi: 10.1016/j.cja.2016.02.005.

[50] F. Demim, A. Boucheloukh, A. Nemra, E. Kobzili, M. Hamerlain, and A. Bazoula, "An adaptive SVSF-SLAM algorithm in dynamic environment for cooperative unmanned vehicles," *IFAC-PapersOnLine*, vol. 52, no. 15, pp. 394–399, 2019, doi: 10.1016/j.ifacol.2019.11.707.

[51] F. Demim, A. Nemra, A. Boucheloukh, E. Kobzili, M. Hamerlain, and A. Bazoula, "SLAM based on adaptive SVSF for cooperative unmanned vehicles in dynamic environment," *IFAC-PapersOnLine*, vol. 52, no. 8, pp. 73–80, 2019, doi: 10.1016/j.ifacol.2019.08.051.

[52] Y. Liu and C. Wang, "A FastSLAM based on the smooth variable structure filter for UAVs," in *Proc. 15th Int. Conf. Ubiquitous Robots (UR)*, Jun. 2018, pp. 591–596, doi: 10.1109/URAI.2018.8441876.

[53] M. Al-Shabi, M. Bani-Yonis, and K. S. Hatamleh, "The sigma-point central difference smooth variable structure filter application into a robotic arm," in *Proc. IEEE 12th Int. Multi-Conf. Syst., Signals Devices (SSD15)*, Mar. 2015, pp. 1–6, doi: 10.1109/SSD.2015.7348201.

[54] M. AlShabi and A. Elnady, "Recursive smooth variable structure filter for estimation processes in direct power control scheme under balanced and unbalanced power grid," *IEEE Syst. J.*, vol. 14, no. 1, pp. 971–982, Mar. 2020, doi: 10.1109/JSYST.2019.2919792.

[55] F. Demim, S. Benmansour, N. Abdelkrim, A. Rouigueb, M. Hamerlain, and A. Bazoula, "Simultaneous localisation and mapping for autonomous underwater vehicle using a combined smooth variable structure filter and extended Kalman filter," *J. Experim. Theor. Artif. Intell.*, vol. 34, no. 4, pp. 621–650, Jul. 2022, doi: 10.1080/0952813x.2021.1908430.

[56] F. Demim et al., "A new adaptive smooth variable structure filter SLAM algorithm for unmanned vehicle," in *Proc. 6th Int. Conf. Syst. Control (ICSC)*, May 2017, pp. 6–13, doi: 10.1109/ICoSC.2017.7958664.

[57] S. Rahimifard, S. Habibi, G. Goward, and J. Tjong, "Adaptive smooth variable structure filter strategy for state estimation of electric vehicle batteries," *Energies*, vol. 14, no. 24, p. 8560, Dec. 2021, doi: 10.3390/en14248560.

[58] H. Zhou, Y. Xia, and Y. Deng, "A new particle filter based on smooth variable structure filter," *Int. J. Adapt. Control Signal Process.*, vol. 34, no. 1, pp. 32–41, Jan. 2020, doi: 10.1002/acs.3067.

[59] M. Avzayesh, M. F. Abdel-Hafez, W. M. F. Al-Masri, M. AlShabi, and A. H. El-Hag, "A hybrid estimation-based technique for partial discharge localization," *IEEE Trans. Instrum. Meas.*, vol. 69, no. 11, pp. 8744–8753, Nov. 2020, doi: 10.1109/TIM.2020.2999165.

[60] M. Attari and S. Habibi, "Automotive tracking technique using a new IMM based PDA-SVSF," in *Proc. ASME Int. Mech. Eng. Congr. Expo. (IMECE)*, 2014, pp. 2–5, doi: 10.1115/IMECE2014-36412.

[61] Y. Chen, L. Xu, G. Wang, B. Yan, and J. Sun, "An improved smooth variable structure filter for robust target tracking," *Remote Sens.*, vol. 13, no. 22, p. 4612, Nov. 2021, doi: 10.3390/rs13224612.

[62] W. Chen, H. Zhou, F. Shen, and Z. Guo, "Current statistic model and adaptive tracking algorithm based on Kalman and smooth variable structure filters," in *Proc. IEEE Int. Conf. Microw. Millim. Wave Technol. (ICMMT)*, vol. 2, Jun. 2016, pp. 1064–1066, doi: 10.1109/ICMMT.2016.7762534.

[63] H. H. Afshari, M. Attari, R. Ahmed, A. Delbari, S. Habibi, and T. Shoa, "Reliable state of charge and state of health estimation using the smooth variable structure filter," *Control Eng. Pract.*, vol. 77, pp. 1–14, Aug. 2018, doi: 10.1016/j.conengprac.2018.04.015.

[64] Y. Tian, H. Suwoyo, W. Wang, and L. Li, "An ASVSF-SLAM algorithm with time-varying noise statistics based on MAP creation and weighted exponent," *Math. Problems Eng.*, vol. 2019, no. 1, pp. 14–20, Jan. 2019, doi: 10.1155/2019/2765731.

[65] J. Goodman, S. A. Wilkerson, C. Eggleton, and S. A. Gadsden, "A multiple model adaptive SVSF-KF estimation strategy," *Proc. SPIE*, vol. 11018, May 2019, Art. no. 110181K, doi: 10.1117/12.2520018.

[66] Y. Qin, Y. Liang, Y. Yang, F. Yang, and X. Wang, "A nonlinear filter switch method based on normalized innovation square," in *Proc. 32nd Chin. Control Conf.*, Jul. 2013, pp. 4719–4724.

[67] R. Piché, "Online tests of Kalman filter consistency," *Int. J. Adapt. Control Signal Process.*, vol. 30, no. 1, pp. 115–124, Jan. 2016, doi: 10.1002/acs.2571.

[68] A. S. Lee, S. A. Gadsden, and S. A. Wilkerson, "An adaptive smooth variable structure filter based on the static multiple model strategy," *Proc. SPIE*, vol. 11018, May 2019, Art. no. 110181D, doi: 10.1117/12.2519771.

[69] M. A. El Sayed and S. Habibi, "Inner-loop control for electro-hydraulic actuation systems," *J. Dyn. Syst., Meas., Control*, vol. 134, no. 1, pp. 1–8, Jan. 2012, doi: 10.1115/1.4001338.

[70] S. Habibi, R. Burton, and E. Sampson, "High precision hydrostatic actuation systems for Micro- and nanomanipulation of heavy loads," *J. Dyn. Syst., Meas., Control*, vol. 128, no. 4, pp. 778–787, Dec. 2006, doi: 10.1115/1.2229259.

[71] K. McCullough, "Design and characterization of a dual electro-hydrostatic actuator," Ph.D. thesis, McMaster Univ., Hamilton, ON, Canada, Tech. Rep., 2011. [Online]. Available: http://hdl.handle.net/11375/9896

[72] J. Goodman, W. Hilal, S. A. Gadsden, and C. D. Eggleton, "Adaptive SVSF-KF estimation strategies based on the normalized innovation square metric and IMM strategy," *Results Eng.*, vol. 16, Dec. 2022, Art. no. 100785, doi: 10.1016/j.rineng.2022.100785.

[73] S. Habibi, "Parameter estimation using a combined variable structure and Kalman filtering approach," *J. Dyn. Syst., Meas., Control*, vol. 130, no. 5, pp. 1–14, Sep. 2008, doi: 10.1115/1.2907393.

[74] A. F. Genovese, "The interacting multiple model algorithm for accurate state estimation of maneuvering targets," *Johns Hopkins APL Tech. Dig. (Appl. Phys. Lab.)*, vol. 22, no. 4, pp. 614–623, 2001.

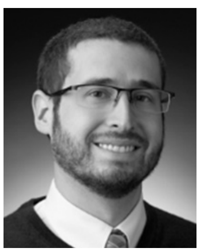

Jacob Goodman received the Ph.D. degree in mechanical engineering in estimation theory from the University of Maryland, Baltimore County, MD, USA, in 2019.

He subsequently joined the John Hopkins University Applied Physics Laboratory (APL), Laurel, MD, USA, in 2019, as an intern. Now, he has transitioned to industry in the Air and Missile Defense Sector.

Waleed Hilal (Student Member, IEEE) received the bachelor's degree in mechanical engineering from the University of Guelph, Guelph, ON, Canada, in 2020, with a dual focus on advanced mechatronic and sustainable energy systems. He is currently pursuing the Ph.D. degree in mechanical engineering and artificial intelligence with McMaster University, Hamilton, ON, Canada.

He is currently a Graduate Research Assistant with the Intelligence and Cognitive Engineering (ICE) Laboratory, Department of Mechanical Engineering, McMaster University. He is also involved in various research projects with industrial partners, such as Adastra Corporation, Toronto, ON, Canada, where he delivers data solutions for industrial applications. His research interests include machine learning techniques for anomaly and fault detection, generative adversarial networks, and cognitive dynamic systems.

Stephen A. Gadsden Sr. (Senior Member, IEEE) received the B.Eng. degree in mechanical engineering and management (business) and the Ph.D. degree in mechanical engineering in estimation theory from McMaster University, Hamilton, ON, Canada, in 2006 and 2011, respectively.

He worked as a Postdoctoral Researcher with the Center for Mechatronics and Hybrid Technology, and a Project Manager in the pharmaceutical industry for three years. He is currently an Associate Professor with the Department of Mechanical Engineering, McMaster University. He was previously an Associate Professor with the University of Guelph, Guelph, ON, Canada, and an Assistant Professor with the University of Maryland, Baltimore County, MD, USA.

Dr. Gadsden is a Distinguished Researcher, having received the 2019–2020 University Research Excellence Award for the College of Engineering and Physical Sciences at the University of Guelph.

Charles D. Eggleton received the B.Sc. degree in naval architecture from the University of California, Los Angeles, Los Angeles, CA, USA, in 1986, and the M.Sc. and Ph.D. degrees in aeronautics and astronautics from Stanford University, Stanford, CA, USA, in 1989 and 1994, respectively.

He became an Assistant Professor with the Department of Mechanical Engineering, University of Maryland, Baltimore County, MD, USA, in 1998. In 2004, he was promoted to an Associate Professor, and then to a Full Professor in 2012. His research interests include deformable particles including biological cells, their mechanical behavior, and the influence of hydrodynamic forces and applied external forces on their behavior.

Dr. Eggleton also served as the Chair of the Department from 2012 to 2018.